HHS Public Access

Author manuscript

Magn Reson Imaging Clin N Am. Author manuscript; available in PMC 2018 November 21.

Published in final edited form as:

Magn Reson Imaging Clin N Am. 2016 February ; 24(1): 187–204. doi:10.1016/j.mric.2015.08.009.

Role of Multiparametric MR Imaging in Malignancies of the Urogenital Tract

Alberto Diaz de Leon, MD, **Daniel Costa, MD**, and **Ivan Pedrosa, MD***

Department of Radiology, University of Texas Southwestern Medical Center, 2201 Inwood Road, 2nd Floor, Suite 202, Dallas, TX, USA

SUMMARY

mpMRI is a useful tool to depict and accentuate biophysical contrasts to yield anatomic and pathophysiologic information about GU malignancies. The role of mpMRI continues to grow due to its ability to detect and characterize GU tumors as well as assess response to treatment. Familiarity with the various imaging techniques and findings allows radiologists to have a significant impact on clinical management of patients with GU malignancies.

Keywords

MR imaging; Diffusion-weighted imaging; Dynamic contrast-enhanced MR imaging; Arterial spin labeling; Kidney cancer; Prostate cancer; Urothelial carcinoma

INTRODUCTION

The term, *mpMRI*, is increasingly used in reference to an approach that takes advantage of the added value of different MR imaging acquisitions to evaluate patients with different tumors, including genitourinary (GU) malignancies. These approaches often include anatomic T1-weighted and T2-weighted images of the region of interest combined with other acquisitions, such as DWI and/ or DCE imaging, to provide information about the tumor microenvironment beyond what can be achieved with any single sequence alone. Appropriately performed, these mpMRI protocols offer anatomic insight and possibly qualitative, semi-quantitative, and fully quantitative imaging bio-markers, which attempt to reflect the underlying tumor histopathology and biological behavior. This is best illustrated in the characterization and risk stratification of renal and prostate masses, grading of ureteral malignancies, and staging of bladder cancer, settings where the radiologist has the opportunity to influence clinical management. Moreover, these methods can be applied to quantitatively monitoring tumor response to therapy.

This review discusses technical aspects and the clinical role of mpMRI protocols in the evaluation of malignancies of the urogenital tract, including the kidney, ureter, bladder, and prostate.

*Corresponding author. ivan.pedrosa@UTSouthwestern.edu.

The authors have nothing to disclose.

MULTIPARAMETRIC MR IMAGING— TECHNIQUES

Most mpMRI protocols share similar imaging strategies, although different sequences may be applied depending on the body part imaged due to anatomic and practical considerations. Imaging the kidneys has inherent challenges resulting from large degree of motion associated with respiration compared with imaging the prostate, for example, which does not move as much. The size of these organs also influences the spatial resolution of the mpMRI acquisitions. Thus, fast, motion-insensitive sequences or motion-compensated strategies with modest spatial resolution are preferred in the abdomen compared with longer, high-resolution scans in the pelvis.

The MR imaging protocols used for the evaluation of renal masses have been discussed elsewhere.[1–5] Examinations can be performed at either 1.5T or 3T, although use of a phased-array body coil is mandatory for an optimal examination. Both 2-D and 3-D acquisitions are used in most renal mass protocols.

Although standard MR imaging protocols for abdominal imaging allow for evaluation of the ureters, a dedicated magnetic resonance (MR) urography (MRU) protocol[4,6–8] offers advantages in the assessment of primary and secondary malignancies involving the ureters. The MRU protocol at the authors' institution is similar to the mpMRI protocol for evaluation of renal masses with the addition of several sequences to optimize visualization of the collecting systems, ureter, and bladder (discussed later).

Dedicated mpMRI protocols for assessment of bladder tumors are less broadly adopted in clinical practice, although they are described else- where.[9–12] Optimal evaluation requires high spatial resolution images with a phased-array surface coil. Dedicated pelvic coils or those with larger number of coil elements over a small anatomic area, such as a cardiac coil, tend to provide better image quality for targeted imaging of the pelvis. The use of an endorectal coil (ERC) for evaluation of bladder base and posterior bladder tumors has also been described elsewhere, although it is not routinely used at the authors' institution.[13]

There are a few unique issues that must be considered when imaging the bladder. Small tumors may be obscured in an underdistended bladder. Bladder overdistention may lead to discomfort, which might result in increased voluntary motion and decreased sensitivity to flat and small tumors. Optimal bladder distention can be achieved by asking the patient to void 2 hours prior to imaging.[9] Assessment of small lesions before and after contrast can be further challenged by progressive filling of the bladder during the MR imaging examination, making the image coregistration difficult. Motion artifacts as a result of bowel peristalsis can degrade images, although administering hyoscyamine (oral or sublingual) or glucagon (intramuscular or intravenous) prior to imaging can be helpful.[14] Finally, chemical shift artifacts at the fat-water interface are commonly encountered when imaging the bladder and can limit evaluation of the bladder wall. Increasing the receiving bandwidth and changing the direction of the frequency-encoding gradient are ways to reduce or displace this artifact, respectively.[15]

The standard sequences in the mpMRI protocol for the evaluation of the prostate have been described elsewhere[16] and are now widely accepted.[17] Currently, there is, however, no

consensus regarding the appropriate choice of hardware when imaging the prostate, specifically regarding whether an ERC should be used.[17] At 1.5T, the use of an ERC is generally supported and is superior to an external coil alone for evaluation of prostate cancer.[18–21] 3T imaging without an ERC is supported by the superior signal-to-noise ratio (SNR) compared with 1.5T scanners, as well as lower costs, improved patient work-flow, and presumed patient acceptance due to discomfort associated with the ERC.[22,23] The reported image quality of 3T MR imaging without ERC is similar that of 1.5T MR imaging using an ERC[24]; however, comparisons of diagnostic performance with both 1.5T and 3T strategies with and without the ERC are lacking.[25]

Prostate imaging is optimized by adequate patient preparation. Patients are asked to avoid ejaculation at least 3 days prior to imaging to increase seminal vesicle distention. In postbiopsy patients, imaging should be avoided, if possible, for at least 6 weeks after the procedure because hemorrhage and architectural distortion may mimic or obscure tumors as well as capsular disruption.[17]

T2-Weighted Sequences

Depending on the organ of interest, T2-weighted spin-echo acquisitions can be obtained using either multishot or single-shot techniques, with or without fat suppression. The authors prefer half-Fourier single-shot turbo spin-echo (HASTE)/single-shot fast spin-echo (SSFSE)/single-shot turbo spin-echo (SSTSE) sequences for T2-weighted imaging of the kidneys and upper GU tract. The fast, sequential acquisitions enabled by these sequences are particularly useful in the upper abdomen where diaphragmatic motion can result in significant image degradation. The addition of fat-suppression strategies helps improve image contrast.

T2-weighted multishot sequences provide the additional benefits of greater image contrast, SNR, and spatial resolution compared with single-shot techniques, although they are more vulnerable to motion artifacts. Multishot techniques can be combined with a variety of respiratory compensation strategies to eliminate or improve motion artifacts, although imaging times are further increased. Novel acquisition strategies, such as those using rotating blades during *k*-space acquisition (eg, Propeller [GE Healthcare, Waukesha, WI], Blade [Siemens Healthcare, Erlangen, Germany], MultiVane [Philips Healthcare, Best, The Netherlands]), are particularly effective in eliminating respiratory-associated artifacts.

Heavily T2-weighted images using long echo times and thick-slice profile acquired in the coronal plane are useful in the evaluation of the collecting system and ureters. These rely on the intrinsic long T2 relaxation time of urine to display hyperintense signal in the GU track against the dark, suppressed background on a single 2-D image. Evaluation of the GU tract is feasible using a variety of 2-D breath-held, thick-slab acquisitions, such as HASTE/ SSFSE/SSTSE or rapid acquisition with relaxation enhancement, as well as respiratory-triggered 3-D fast spin-echo (FSE)/ turbo spin-echo sequences. Fat saturation techniques can provide additional optimization in the background suppression. Volumetric acquisitions help evaluate complex anatomy and pathology using multiplanar reconstructions and 3-D reformations, such as maximum intensity projection and volume rendering. In contrast, the short acquisition time (ie, approximately 2 seconds per image) of 2-D acquisitions offer the

opportunity to create cinelike acquisitions, which can be helpful in distinguish areas of ureteral peristalsis from true pathology (ie, stenosis).

Multiplanar high-resolution, free-breathing, T2-weighted multishot FSE images are preferred for evaluation of malignancies in the bladder. A saturation band placed over the subcutaneous fat in the anterior abdominal wall can help mitigate respiratory ghosting artifacts, although caution must be taken to avoid obscuring the anterior bladder. Other respiratory compensation strategies and alternative *k*-space acquisitions, such as rotating blades in *k*-space, may be useful although usually require longer acquisition times. Patient motion artifacts can still be problematic in some cases and may necessitate use of motion-insensitive SSFSE techniques. Steady-state free-precession sequences provide images with very high SNR where fluid and blood vessels are hyperintense, although limited by off-resonance artifacts when applied to a large field of view. The addition of fluid-attenuated inversion recovery strategies has been advocated to achieve T2-weighted evaluation of tumorswhilesuppressinghyperintenseurinesignal.[26]

Assessment of patients with known or suspected prostatic cancer requires high-resolution, small field of view (eg, 180–220 mm) multiplanar T2-weighted FSE images, with axial images considered the workhorse for depiction of anatomy with optimal distinction between the intermediate-to-high signal intensity of the peripheral zone and the heterogeneous, high and low signal intensity of the central gland in most patients. These images are also the most important to assess extraprostatic extension in most patients. Coronal and sagittal images can be included to help distinguish nodular features of benign prostatic hypertrophy (BPH) from ill-defined tumors as well as wedge-shaped abnormalities in prostatitis. These can also help in the assessment of areas suspicious for extraprostatic or seminal vesicle invasion. An FSE acquisition with an echo time between 90 to 120 ms provides optimal soft-tissue contrast for delineation of prostatic cancers against the hyperintense peripheral zone.[27,28] Detection of extraprostatic extension may be improved with the utilization of a 3-D FSE acquisition with isotropic voxel resolution.[29] A quantitative approach has been recently proposed with a whole-gland T2 mapping using a multiecho T2-weighted FSE sequence in approximately 6 minutes.[30] Although the role of this type of acquisition has not been yet established, it provides an opportunity to explore additional quantitative measures of tumor characteristics in the context of mpMRI of the prostate.

T1-Weighted Sequences

When imaging the abdomen, the use of gradient-recalled echo (GRE) techniques for the acquisition of T1-weighted images provides rapid imaging (ie, full renal coverage in 15–20 seconds) with an adequate SNR. Depending on the selection of imaging parameters, these images can serve a variety of roles, including, but not limited to, the detection of lipids and noncontrast assessment for vessel patency.

2-D GRE T1-weighted in-phase (IP) and opposed-phase (OP) images, or chemical shift imaging, of the abdomen are used in the renal mass and MRU protocols for the detection of intravoxel lipids. Recently developed 3-D dual-echo Dixon-based acquisitions allow for acquisition of thinner, contiguous slices in a single breath-hold that can then be reconstructed into water, fat, IP, and OP imaging data sets. The thinner slices allow for

detection of smaller amounts of intratumoral lipids. Alternatively, Dixon-based sequences with multiple echoes (eg, 6 echoes) offer a way to not only detect but also quantify intralesional lipids, which may provide additional information about tumor biology (Fig. 1).

Determination of the tissue T1-relaxation time (T1-mapping) may be necessary when performing quantitative analysis of DCE data sets. There are different strategies to accomplish this, such as separate T1 acquisitions obtained with the same parameters as those for the DCE protocol but with variable flip angles (eg, 2°, 5°, and 10°), Look-Locker acquisitions, and modified Look-Locker acquisitions.[31]

Contrast-Enhanced Imaging

Although the terms, *DCE MR imaging and multiphasic contrast-enhanced (MCE) MR imaging*, are often used interchangeably, these refer to different imaging acquisition strategies. MCE MR imaging and CT are analogous in that images are acquired during specific phases, usually at 2 to 4 specific times after the contrast administration. MCE MR imaging protocols are based on lower temporal, higher spatial-resolution acquisitions, which provide some level of temporal information while maintaining the high spatial resolution needed for characterization of disease and treatment planning in clinical practice. This method is best typified by renal imaging (ie, corticomedullary, nephrographic, and excretory phases) and is used to provide a qualitative assessment of enhancement characteristics of a specific organ and/or pathophysiologic condition.

DCE MR imaging involves a lower spatial, higher temporal resolution strategy during the acquisition of multiple serial images before, during, and after intravenous injection of gadolinium to provide a more detailed, quantitative, and/or semiquantitative pharmacokinetic assessment of enhancement. This technique is most often used in the evaluation of prostate masses and, to a lesser extent, renal masses and bladder tumors. Accurate quantitative assessment of enhancement characteristics in a tumor usually requires high temporal resolution imaging, because it allows for the acquisition of a greater number of images. This may be dependent, however, on the intrinsic pathophysiologic characteristics of the tumor.

For example, the vascularity in the prostate and in prostate cancer is low compared with that of the kidneys and renal cancer, respectively. Thus, a higher temporal resolution may be necessary for assessment of renal masses than that of prostate cancer. MCE MR imaging with high spatial resolution offers a semiquantitative, although potentially less accurate, description of enhancement characteristics.[32]

Kidney

At the authors' institution, 3-D fat-suppressed spoiled gradient echo (SPGR) T1-weighted sequences are acquired in the coronal plane. The water reconstruction of Dixon-based acquisitions is preferred because of the more robust, homogeneous fat suppression compared with frequency-selective fat saturation strategies, particularly at high field strength (ie, 3T). A semiquantitative assessment of renal mass enhancement is accomplished by an acquisition during the corticomedullary phase (timed to the arrival of contrast to the kidneys with an MR imaging fluoroscopic technique) followed by images obtained during the early (ie, 40 s)

and late (ie, 90 s) nephrographic phase. Sagittal oblique images of each kidney and axial images are obtained during the excretory phase.

A more quantitative assessment of vascularity in renal masses is feasible using a DCE MR imaging protocol, although respiratory motion and the needs for anatomic coverage may dictate the acquisition strategy. An acquisition of a single slice through the renal mass with a saturation prepared 2-D T1-weighted acquisition provides a motion-insensitive (ie, free breathing) and a very fast (<2 s) temporal resolution[33]; however, this approach provides limited tumor coverage. Alternatively, a 3-D acquisition with a SPGR sequence provides an assessment of the entire tumor although with lower temporal resolution and, thus, generally incompatible with free-breathing acquisitions. The authors prefer the whole-tumor assessment using a 3-D SPGR acquisition with a 5-second temporal resolution acquired in groups of 3 sets of images within a 15-second breath-hold. These are alternated with 15-second periods for breathing over a 6-minute total acquisition time. Newer acquisitions using alternative *k*-space filling approaches, such as different versions of *k*-hole, radial, spiral, and view-sharing strategies, may provide the opportunity to obtain high-quality, free-breathing, whole-tumor DCE data sets.

Ureter

Neoplasms arising from or involving the ureters are usually evaluated with an MCE MR imaging protocol and qualitative assessment of enhancement characteristics. The authors use an magnetic resonance urography (MRU) protocol, which comprises the same MCE acquisitions as that of the renal mass protocol, with the addition of an excretory phase acquisition, which is typically obtained 5 minutes after intravenous contrast administration. When using a standard dose of contrast, concentrated gadolinium in urine results in dark signal intensity due to T2* effects. The intravenous administration of 5 to 10 mg of furosemide prior to injection of gadolinium facilitates the evaluation of the collecting system by increasing water excretion and distention of the collecting system as well as dilution of the concentrated gadolinium, which becomes hyperintense.[34,35] Although administration of a low-dose of gadolinium has also been suggested, MRU in the absence of a pharmacologic diuresis is limited by lack of distention of the collecting system.[36]

Bladder

The use of DCE MR imaging or MCE MR imaging approaches for assessment of bladder tumors varies among institutions, because the utility remains controversial.[37] MCE MR imaging acquisitions may provide a better delineation of the tumor extension in some patients, although local staging is usually based on high-resolution T2-weighted images. A single-slice, high-temporal resolution DCE protocol has been proposed for the characterization and staging of bladder cancer.[38] This approach is not widely used, however, in clinical practice, mainly due to limited anatomic coverage to assess the entire tumor. Again, the newly developed 3-D T1-weighted acquisitions may offer an opportunity to assess the whole-tumor with quantitative DCE MR imaging, although the experience with these techniques is still limited.

Prostate

A detailed discussion of DCE imaging of the prostate and the various means of analysis (ie, kinetic compartmental modeling) is beyond the scope of this review. DCE MR imaging of the prostate is accomplished with a 3-D T1-weighted SPGR sequence covering the entire prostate and acquired before, during, and after the administration of a single dose of a gadolinium-based contrast agent administered at 2 to 4 mL/s followed by a 20-mL saline flush.[39] Images are acquired repeatedly for at least 5 minutes. There is debate about the optimal temporal resolution of DCE MR imaging acquisitions. A temporal resolution of 5 to 10 seconds (no more than 15 seconds) has been proposed for quantitative assessment of DCE data sets.[39] Faster 3-D acquisitions are possible and may provide an improved delineation of prostate tumors.[40]

Several models have been proposed to analyze DCE image data sets, with the 2-compartment Tofts model representing the most commonly applied.[41] There is no consensus, however, regarding the best approach to analyze DCE MR imaging results.[17] The authors use a commercially available postprocessing software for qualitative, quantitative, and semiquantitative analysis, for expedited review and increased consistency.[16] Optimal results have been reported using a 3-D acquisition with higher spatial resolution but much slower temporal resolution using a semiquantitative 3 time-point approach for data analysis.[42]

Diffusion-Weighted Imaging

The technical parameters for DWI, including method of acquisition (FSE, gradient-echo, line scan, echo-planar imaging [EPI], and so forth), breath-hold versus respiratory compensated versus free-breathing imaging, and optimal number of b-values, vary depending on the anatomic region of interest. In general, fat suppression is considered essential to avoid chemical shift artifacts for all body applications. Additionally, parallel imaging is often used to achieve a shorter echo time, thereby increasing SNR and decreasing the echo train, thus reducing geometric distortion related to susceptibility artifacts.[43]

Breath-hold DWI with a single-shot EPI technique allows for rapid image acquisition and reduction in motion artifact. Only a few b-values and/or number of signal averages can be obtained within the duration of a breath-hold; thus, these acquisitions suffer from poor SNR, which only worsens with higher b-values. Limited SNR frequently results in poor fitting of the data when calculating ADC maps.

Free-breathing techniques with multiple signal averages are associated with longer acquisition times, although there are benefits from greater SNR, contrast-to-noise ratio, and the ability to acquire a greater number of b-values. Alternatively, images can be acquired with respiratory compensation strategies, such as respiratory triggering with abdominal bellows or pencil-beam navigators. For clinical MR imaging examinations, the authors rely on abdominal bellows for respiratory compensation because of the time efficiency of this approach compared with navigator-triggered acquisitions. Although navigator-triggered acquisitions tend to offer more robust slice registration, the inherent long acquisition times prohibit their broad implementation in clinical practice.

As is true for many other applications, there are no standardized protocols for DWI of the urinary tract. Free-breathing, breath-hold, and respiratory triggered sequences have been proposed and a wide range of number and levels of b-values reported. The number of b-values acquired is based on a balance between the total acquisition time and the need for reliable fitting of the data for generating ADC maps. In general, a larger number of b-values may improve the quality of the fitting for the ADC calculation, although other factors, such as respiratory motion and SNR (ie, at higher b-values), must be taken into consideration. The selection of b-values is also influenced by the type of acquisition and body part. As the b-value increases, signal from water molecules decreases, as does the SNR. Most manufacturers allow for a different number of signal averages(NSA)/excitations (NEX) for each b-value permitting them to increase the SNR for the higher b-values by adding more averages while obtaining less averages for lower b-values, thus maintaining the total acquisition time as short as possible. The authors use the following strategy to select the number of signal averages for each b-value: 1 acquisition for b-values between 0 and 499; 2 acquisitions for b-values between 500 and 999; 3 acquisitions for b-values between 1000 and 1499; and 4 acquisitions for b-values between 1500 and 2000. In some cases the number of averages may need to be modified depending on the clinical indication, magnet field strength (ie, 1.5T vs 3T), and coil characteristics (ie, endorectal plus phased-array coil vs phased-array alone).

Regarding the selection of b-values, the authors use a respiratory-triggered DWI acquisition with 4 b-values when imaging the upper abdomen: 0 s/mm^2, 50 s/mm^2, 400 s/mm^2, and 800 s/mm^2. Many variations of this protocol have been reported and may be considered in specific applications. Similarly, for evaluation of the prostate, an optimal b-value has not been established. The European Society of Urogenital Radiology suggests the use of 3 b-values: 0 s/mm^2, 100 s/mm^2, and 800 to 1000 s/mm^2.[44] It has recently been suggested that higher b-values (1000–2000 s/mm^2) allow for improved cancer detection, particularly in the transitional zone.[45–47] Parallel imaging and a higher band-width are recommended when using a single-shot EPI DWI technique to help overcome spatial distortion related to magnetic field inhomogeneities caused by air in the rectum or in the ERC.[48–50]

Arterial Spin-Labeled MR imaging

ASL is a method for quantitatively assessing blood flow to a region of interest by using arterial water as an endogenous contrast agent.[15] Arterial hydrogen protons are labeled using a radiofrequency inversion pulse and allowed to enter the imaging plane. Quantitative ASL perfusion maps can be created after subtraction of images acquired without and with labeling and provide a measurement of tissue perfusion in milliliters per 100 g of tissue per minute.[51–54] Because the signal difference between label and control images is usually small (ie, approximately 2% for brain studies), ASL acquisitions are relatively SNR poor and relay on multiple signal averages. ASL has been extensively studied in brain applications, although its use in GU pathology is increasing and discussed in detail later. Different versions of ASL imaging have been implemented and applied in the kidneys with different labeling strategies. Among these are pulsed ASL acquisitions, such as flow-sensitive alternating inversion recovery and pseudocontinuous ASL acquisitions, the latter offering a more efficient labeling strategy and therefore superior SNR compared with pulsed ASL

approaches. Similarly, different ASL readout strategies are available for assessment of renal perfusion and diseases, such as single-slice, multislice, and 3-D acquisitions.

Blood Oxygen Level–Dependent MR Imaging

Blood oxygen level–dependent (BOLD) MR imaging is a type of acquisition used to assess tissue oxygenation by using the paramagnetic properties of deoxyhemoglobin.[55,56] Changes in deoxyhemoglobin concentration result in generation of phase incoherence of magnetic spins and signal attenuation, and this difference in signal is reflected on T2*-weighted gradient-echo sequences. The utility of BOLD MR imaging has recently been reported for the characterization of renal masses and subtyping of RCC,[57,58] although differences among various histopathologic subtypes may be related to T2* effects associated, for example, with iron (ie, hemosiderin) deposition in the tumor instead of differences in oxygenation levels. Data regarding the use of BOLD to evaluate urinary tract malignancies before and after chemotherapeutic interventions are still lacking.

Magnetic Resonance Spectroscopy

In MR spectroscopy (MRS), resonant frequencies unique for protons in different metabolites are reflected by its respective position on an output graph. The strength of the MR signal is proportional to the number of protons at that frequency. Its role in the evaluation of the urinary tract remains largely investigational. In the kidney, studies have shown that MRS in metastatic RCC (mRCC) demonstrate a significantly lower ratio of signal at a 5.4-ppm frequency shift to that at 1.3 ppm (the latter may be correlated with the lipid content in the voxel) compared with that in healthy tissue.[59,60] In the prostate, the primary metabolites of interest are choline and citrate. Normal prostatic epithelial cells synthesize and secrete citrate.[61] Accordingly, citrate is decreased in the setting of prostate cancer, which is thought to be due to both loss of normal cellular function and luminal morphology/organization.[62,63] Choline, a marker of cell turnover, is elevated in prostate cancer.[64] Despite its potential as a metabolic biomarker in GU cancer, MRS is rarely used in clinical practice due to difficult implementation (eg, common technical failures) with the exception of a few centers with specific expertise in this technique.

CLINICAL APPLICATIONS

Kidney

MR imaging can play an important role in the evaluation of renal masses by providing an opportunity to reliably diagnose benign tumors, such as classic angiomyolipomas, containing bulk adipose tissue. MR imaging can also narrow the differential diagnosis in patients with suspected angiomyolipomas without visible fat, facilitating the recommendation to proceed with a diagnostic percutaneous biopsy and thereby avoid an unnecessary surgery. In some instances, MR imaging allows for a specific histopathologic diagnosis and even tumor grading in patients with RCC. Because of the lack of ionizing radiation, MR imaging may play an important role also in patients on active surveillance and those followed with serial imaging after treatment.

Mass characterization and subtyping of renal cell carcinoma

The noninvasive determination of a tumor subtype can have considerable therapeutic implications. Chemotherapeutic options can be appropriately tailored in those who are poor surgical candidates or have metastatic disease.[65,66] Alternatively, subtyping may be helpful to the urologist for operative planning in surgical candidates.

The 3 most common subtypes of RCC include clear cell RCC (ccRCC, 65%–80%), papillary RCC (pRCC, 10%–15%), and chromophone RCC (chrRCC, 4%–11%).[67,68] These subtypes can be differentiated based on certain imaging characteristics using an mpMRI protocol.[7,69]

ccRCC is a heterogeneous tumor with variable signal intensity on T1-weighted and T2-weighted images, although it frequently displays hyperintense signal on T2-weighted images. ccRCC is a hypervascular tumor and can be differentiated from other histopathologic forms of RCC based on the enhancement characteristics.[70] The average enhancement of ccRCC during the corticomedullary phase is approximately 200% compared with 30% for pRCC and 110% of chrRCC.[70] ccRCC tends to exhibit enhancement similar to or higher than that of the renal cortex (ie, tumor-to-cortex ratio 1.4).[70] On ASL, ccRCC demonstrates high blood flow levels (171.6 mL/ min/100 g 61.2) (Fig. 2).[71] The presence of a central area of no enhancement, retroperitoneal collateral vessels, and venous invasion is associated with high-grade tumor.[69] Intracytoplasmic deposition of lipids is distinctive of ccRCC and results in a characteristic appearance on IP/OP imaging with moderately high signal intensity on T1-weighted images relative to the renal cortex demonstrating a decrease in signal intensity on OP imaging.[4,7,69] The combination of intravoxel lipids on OP imaging, a central area of no enhancement, and avid corticomedullary enhancement is highly specific of ccRCC. Cystic variants of ccRCC do occur and manifest as a complex, predominantly cystic mass with irregular, nodular and septal avid enhancement, a presentation shown to be highly specific (94%) for low-grade ccRCC.[69] Interruption of the tumor pseudocapsule suggests locally advanced disease and a high nuclear grade.[72]

pRCC shows a lower signal intensity relative to the renal cortex on T2-weighted in the viable (ie, vascularized) portions of the tumor and favors a peripheral location in the kidney.[7,69,73,74] This subtype of RCC enhances to a lesser degree and progressively after contrast administration compared to ccRCC and chrRCC.[70] Tumor hemorrhage is common and illustrated by hyperintense signal on T1-weighted images. Like ccRCC, pRCC can manifest as a complex cystic mass, though the presence of hemorrhagic contents and peripheral, hypoenhancing nodules favor the papillary subtype.

pRCC is classified histopathologically into type 1 (basophilic) and type 2 (eosinophilic), with the latter demonstrating worse prognosis.[74] Two distinct imaging subtypes of pRCC have also been described, focal and infiltrating.[75] Infiltrating pRCC is a subtype of type 2 pRCC that carries a much worse prognosis than that of focal pRCC tumors (i.e. both pathologic type 1 or 2), and the association of an infiltrative phenotype with worse prognosis is independent of tumor size and stage.[75] Infiltrating type 2 pRCC is frequently associated with venous invasion. Regardless of its presentation, viable portions of the tumor in pRCC are almost always hypoenhancing during the corticomedullary phase (ie, approximately 20% of that of the renal cortex),[70] with rare exceptions showing enhancement approaching 50%

or higher. Similarly, the blood flow levels of pRCC on ASL are lower (27.0 mL/min/100 g ± 15.1) than that of other RCC subtypes (Fig. 3).

The variable, nonspecific imaging characteristics of chrRCC complicates accurate presurgical diagnosis. chrRCC may be hypointense to hyperintense to renal cortex on T2-weighted images and should be suspected in the setting of a large (>4 cm) renal mass, which shows moderate corticomedullary (ie, approximately 50–60% of that of the renal cortex) homogeneous enhancement during the corticomedullary phase[70] without a central area of no enhancement.

Evaluation for therapeutic response in metastatic renal cell carcinoma

Traditional means for evaluating treatment response are based on size criteria (for example, response evaluation criteria in solid tumors (RECIST), version 1.1]).[76] Optimal response to newer systemic, antiangiogenic agents can manifest, however, as changes in tumor vascularity with or without obvious size change.[77,78] This is further complicated by the occurrence of pseudo-progression, the phenomenon of transient, subacute imaging changes in a tumor mimicking progression. MCE MR imaging is well suited for the evaluation of these unusual patterns of treatment response and provides an opportunity for qualitative assessment of the degree of enhancement.

Quantitative measurements of tumor perfusion in DCE MR imaging are also possible, including intratumoral vascular fraction, tumor blood flow, vascular permeability-surface area product and accessible extravascular-extracellular space.

K^{trans} is a commonly cited measure of interest, a parameter describing the transfer constant between the intravascular and extravascular space. A change greater than 40% in K^{trans} from baseline to follow-up has been proposed as consistent with a drug effect in pharmacodynamic studies.[79] Two reports evaluating K^{trans} in sorafenib-treated mRCC patients have offered somewhat divergent conclusions. In 15 patients treated with sorafenib in a phase II study, K^{trans} decreased significantly during treatment (60.3%) and both K^{trans} at baseline and the decrease in K^{trans} after therapy were significantly associated with progression-free survival.[80] These patients had higher response rates and time to progression, however, than the overall rates in phase II studies. In another report, changes in K^{trans} and the area under the contrast concentration versus time curve 90 seconds after contrast injection in mRCC patients correlated with the administered dose of sorafenib, indicating its usefulness as a pharmacodynamic biomarker, although these 2 variables did not correlate with progression-free survival and, therefore, were not considered predictive biomarkers.[81] The investigators indicated, however, a potential association between high baseline K^{trans} and a prolonged time to progression or death.[81]

The relative contribution to signal intensity of both blood flow and vascular permeability in DCE MR imaging, however, complicates the assessment of tumor response to targeted therapies. ASL provides an alternative quantitative, reproducible means for directly assessing tumor blood flow. The lack of contrast administration and the virtually negligible contribution of vascular permeability to the measurements of tissue perfusion are potential advantages of ASL over DCE MR imaging.[82] In a trial of patients with mRCC receiving an

antiangiogenic drug (Vatalanib, Novartis Pharmaceuticals, East Hanover, New Jersey, and Schering AG, Berlin, Germany), early changes at 1 month in blood flow on ASL and tumor size were compared with tumor size changes at 4 months. ASL blood flow changes at 1 month were correlated significantly with time to progression, whereas tumor size changes were not.[83] No correlation was observed between blood flow changes and tumor size changes at 1 month. Similar changes in tumor vascularity can be seen with other antiangiogenic drugs (Fig. 4).

Ureter and Collecting System

The role of MR imaging in screening patients at risk for urothelial neoplasms has not yet been systematically studied. MR imaging remains infrequently used as the primary diagnostic test for hematuria and assessment for upper tract urothelial carcinoma due to its insensitivity to reliably detect and distinguish urinary tract calculi and air.

Nevertheless, MRU continues to evolve and remains a viable option due to its excellent contrast resolution and lack of ionizing radiation for evaluation of patients with known or suspected urothelial carcinoma, the most common primary malignant ureteral neoplasm. In patients unable to receive contrast, it has been suggested that the combination of T2-weighted images and DWI alone are as sensitive as a contrast-enhanced MRU for the detection of undiagnosed upper tract urothelial carcinoma.[84] MRU has been shown more sensitive and specific than noncontrast CT for the diagnosis of causes of urinary tract obstruction other than urolithiasis.[85,86] In a single report of patients with known urothelial carcinoma, MR imaging was found superior to CT for staging these tumors.[87]

Urothelial carcinoma can be multifocal and can present as a sessile intraluminal filling defect or a focus of irregular wall thickening and enhancement.[88,89] Compared with skeletal muscle, urothelial carcinoma is isointense on T1-weighted images and hyperintense on T2-weighted images and is lower in signal intensity relative to urine on T2-weighted images, allowing for its identification in a dilated collecting system/ureter.

In the setting of urothelial carcinoma, proliferation of benign fibrous tissue in the wall of the ureter results in ureteral wall thickening. MR imaging is able to distinguish this reactive, benign wall thickening from malignant invasion, because the latter is relatively hypoenhancing compared with avidly enhancing fibrous tissue.[87,89] Disruption, or fragmentation, of this rim of avid enhancement is helpful in tumor staging because it suggests invasion beyond the muscularis layer (ie, at least T3).[90]

The ADC value of urothelial carcinoma may serve as a potential predictor of its histopathologic grade (Fig. 5). Prior studies have shown an inverse relationship between ADC values and histologic grade and likelihood of metastatic potential.[91,92] ADC values of upper urinary tract urothelial carcinoma have also been shown to be inversely correlated with Ki-67, a marker of cell proliferation and prognostic biomarker for bladder cancer described in detail later.[92]

Bladder

The role of MR imaging in the evaluation of bladder cancer is primarily in local staging. MR imaging has been shown more accurate than CT in demonstrating intramural invasion and extravesicular extension.[12] Bladder carcinoma is staged using the TNM staging system, and T staging is based on the degree of bladder wall invasion. Preoperative distinction between T1 and T2, or greater, stages of disease is vital in guiding management. For T1 disease, a transurethral resection is performed; for stages T2 and above, a partial or total cystectomy and adjuvant therapies are provided.

Bladder carcinoma can present as a sessile or pedunculated endoluminal soft tissue mass of variable signal intensity, although typically hyperintense to detrusor muscle on T2-weighted images. On early postcontrast images, tumor, mucosa, and submucosa enhance to a similar degree; tumor can be distinguished from the surrounding hypointense urine and relatively hypoenhancing detrusor during this phase.[12,37]

Tumor staging is primarily based on high-resolution T2-weighted images although both DCE and DWI may be helpful. Alone, T2-weighted images and DCE images have limited sensitivity of 40% to 67% and 52% to 85%, respectively.[12,37,93–95] In patients with T1 disease, tumor presents as a superficial sessile or papillary mass. On T2-weighted images, the hypointense muscular layer remains uninterrupted, smooth, and hypointense. Tenting of the surrounding bladder wall may or may not be present. Submucosal thickening often accompanies these findings, although it confounds accurate staging, because this finding may be reactive (ie, inflammatory change and/or fibrosis) or represent muscle invasion.

On postcontrast images, however, inflammatory tissue and fibrosis enhance similarly to detrusor muscle, after peak tumor enhancement. In patients who have undergone a bladder biopsy, high temporal resolution DCE imaging may assist in differentiating bladder cancer from postbiopsy inflammatory/granulation tissue because tumors enhanced faster than the latter.[38] Additionally, DWI has been shown to accurately delineate tumor from normal detrusor muscle and distinguish benign submucosal thickening from tumor; cancer is hyperintense compared with muscle and benign inflammatory change or fibrosis.[93,94,96,97] Hyperintense detrusor muscle signal underlying tumor on T2-weighted and/or DWIs suggests muscle invasion.[98] Muscle invasion can also be inferred when there is ureteral dilatation to the level of an ureteropelvic junction bladder tumor.

Similar to urothelial carcinoma of the ureter, DWI and ADC values may play a role in predicting histologic grade and potential treatment response. ADC values correlate inversely with tumor size, histologic grade, and T stage in bladder cancer, in addition to Ki-67, a marker of cell proliferation and prognostic biomarker for bladder cancer.[99] The latter may be a more significant prognostic indicator than histologic grade and pathologic nodal status.[100,101] Prior studies have also shown an association between a higher Ki-67 level and favorable chemoradiosensitivity in bladder cancer, suggesting that lower ADC values may indicate a greater likelihood for treatment response.[102] Similarly, primary bladder tumors with earlier and more avid enhancement on DCE MR imaging are associated with a greater risk of local recurrence after resection.[103]

Prostate

The role of mpMRI in the evaluation of prostate cancer has rapidly evolved since its original inception. Initially limited to disease staging in patients with a known diagnosis of prostate cancer, MR imaging is now accepted as the most accurate imaging technique for detection and localization of cancer in the prostate.[104,105] Preoperative imaging for disease localization may help determine whether nerve-sparing surgery or focal therapies can be pursued.[106–108] The development of MR imaging–transrectal ultrasound (TRUS) image fusion software has further expanded the utility of MR imaging in evaluating patients with rising prostate-specific antigen (PSA) levels and prior negative systematic TRUS biopsies.[109,110] MR imaging–TRUS fusion biopsy of the prostate increases detection of clinically significant prostate cancer while reducing detection of insignificant disease, allowing for a more reliable risk stratification of biopsy-naïve patients and those with known cancer (eg, active surveillance patients).[111]

Prostate carcinoma occurs more commonly in the peripheral zone (70%) than the transitional (20%) and central zones (10%). On T2-weighted images prostate cancer is visualized as an apparent focus of hypointensity relative to the background high signal intensity peripheral zone.[112] On T1-weighted images, prostate cancer is isointense to surrounding prostatic tissue. T1-weighted images are also helpful in distinguishing hyperintense postbiopsy hematoma (commonly hypointense on T2-weighted images) from tumor. On DCE images, rapid enhancement and washout are characteristic of prostate carcinoma.

On DWI, tumors show restricted diffusion with ADC values lower than benign or normal prostatic tissue (Fig. 6).[113] A few studies have shown an inverse relationship between ADC values and tumor aggressiveness. ADC values less than 0.6 10^{-3} mm^2/s increase the likelihood of aggressive disease (Gleason 4) (Fig. 7), although substantial overlap in ADC values exists among tumors with different Gleason scores.[114,115] Additionally, in patients undergoing active surveillance, ADC values may serve as a biomarker of tumor progression and likelihood of the need for treatment intervention.[116,117]

When staging prostate cancer, the primary question to answer is whether the tumor is organ confined (stage T1 or T2) or has extended beyond the prostate pseudocapsule (stage T3 and above). Findings characterizing organ-confined and extracapsular disease have been discussed extensively.[16]

Standardization

The general frame-work for radiology reporting is said to consist of structured format, consistent content, and standard language.[118] This framework is best typified in breast imaging, where report vocabulary and organization are strongly influenced by the Breast Imaging Reporting and Data System (BI-RADS) lexicon. Lack of guidelines and significant variability in interpretation, however, continue to represent challenges for prostate MR imaging.[119] Efforts to improve consistency of interpretation include the development of Prostate Imaging Reporting and Data System (PI-RADS),[17] endorsed by the European Society of Urogenital Radiology and the American College of Radiology, and

implementation of Likert scales.[119,120] In short, PI-RADS version 2 is a scoring scheme that assigns a value, between 1 and 5, to a focal prostate lesion based on strict criteria about the appearance of the lesion on T2-weighted imaging, DWI, and DCE to convey the likelihood of malignancy.[17] The larger the score, the greater the likelihood of malignancy. The authors use a Likert scale scoring system and report templates dividing the peripheral zone in 12 sectors (base, midgland, or apex—medial or lateral and right or left) and the anterior gland in 6 sectors (base, midgland, or apex—right or left).[121]

REFERENCES

1. Allen BC, Tirman P, Jennings Clingan M, et al. Characterizing solid renal neoplasms with MRI in adults. Abdom Imaging 2014;39(2):358–87. [PubMed: 24446014]
2. Nikken JJ, Krestin GP. MRI of the kidney-state of the art. Eur Radiol 2007;17(11):2780–93. [PubMed: 17646992]
3. Ramamurthy NK, Moosavi B, McInnes MD, et al. Multiparametric MRI of solid renal masses: pearls and pitfalls. Clin Radiol 2015;70(3):304–16. [PubMed: 25472466]
4. Sun MR, Pedrosa I. Magnetic resonance imaging of renal masses. Semin Ultrasound CT MR 2009; 30(4):326–51. [PubMed: 19711644]
5. Zhang J, Pedrosa I, Rofsky NM. MR techniques for renal imaging. Radiol Clin North Am 2003;41(5): 877–907. [PubMed: 14521200]
6. Lee KS, Zeikus E, DeWolf WC, et al. MR urography versus retrograde pyelography/ureteroscopy for the exclusion of upper urinary tract malignancy. Clin Radiol 2010;65(3):185–92. [PubMed: 20152273]
7. Pedrosa I, Sun MR, Spencer M, et al. MR imaging of renal masses: correlation with findings at surgery and pathologic analysis. Radiographics 2008; 28(4):985–1003. [PubMed: 18635625]
8. Rothpearl A, Frager D, Subramanian A, et al. MR urography: technique and application. Radiology 1995;194(1):125–30. [PubMed: 7997538]
9. Barentsz JO, Ruijs SH, Strijk SP. The role of MR imaging in carcinoma of the urinary bladder. AJR Am J Roentgenol 1993;160(5):937–47. [PubMed: 8470608]
10. Mallampati GK, Siegelman ES. MR imaging of the bladder. Magn Reson Imaging Clin N Am 2004; 12(3):545–55, vii. [PubMed: 15271370]
11. Teeger S, Sica GT. MR imaging of bladder diseases. Magn Reson Imaging Clin N Am 1996; 4(3): 565–81. [PubMed: 8873020]
12. Tekes A, Kamel I, Imam K, et al. Dynamic MRI of bladder cancer: evaluation of staging accuracy. AJR Am J Roentgenol 2005;184(1):121–7. [PubMed: 15615961]
13. Sugimura Y, Hayashi N, Yamashita A, et al. Endorectal magnetic resonance imaging of the prostate and bladder. Hinyokika Kiyo 1994;40(1):31–6. [PubMed: 7509118]
14. Winkler ML, Hricak H. Pelvis imaging with MR: technique for improvement. Radiology 1986; 158(3):848–9. [PubMed: 3945763]
15. Lawler LP. MR imaging of the bladder. Radiol Clin North Am 2003;41(1):161–77 (0033–8389 (Print)). [PubMed: 12630691]
16. Costa DN, Pedrosa I, Roehrborn C, et al. Multiparametric magnetic resonance imaging of the prostate: technical aspects and role in clinical management. Top Magn Reson Imaging 2014; 23(4):243–57. [PubMed: 25099562]
17. ACR. MR Prostate Imaging Reporting and DataSystem version 2.0 Available at: http://www.acr.org/Quality-Safety/Resources/PIRADS/. Accessed June 12, 2015.
18. Amis ES, Jr, Bigongiari LR, Bluth EI, et al. Pretreatment staging of clinically localized prostate cancer. American College of Radiology. ACR Appropriateness Criteria. Radiology 2000; 215(Suppl):703–8. [PubMed: 11037488]
19. Engelbrecht MR, Jager GJ, Laheij RJ, et al. Local staging of prostate cancer using magnetic resonance imaging: a meta-analysis. Eur Radiol 2002; 12(9):2294–302. [PubMed: 12195484]

20. Hricak H, Jager GJ, Laheij RJ, et al. Carcinoma of the prostate gland: MR imaging with pelvic phased-array coils versus integrated endorectal– pelvic phased-array coils. Radiology 1994;193(3): 703–9. [PubMed: 7972810]
21. Schnall MD, Imai Y, Tomaszewski J, et al. Prostate cancer: local staging with endorectal surface coil MR imaging. Radiology 1991;178(3):797–802. [PubMed: 1994421]
22. Heijmink SW, Fütterer JJ, Hambrock T, et al. Prostate cancer: body-array versus endorectal coil MR imaging at 3 T–comparison of image quality, localization, and staging performance. Radiology 2007;244(1):184–95. [PubMed: 17495178]
23. Lee SH, Park KK, Choi KH, et al. Is endorectal coil necessary for the staging of clinically localized prostate cancer? Comparison of non-endorectal versus endorectal MR imaging. World J Urol 2010;28(6):667–72. [PubMed: 20623288]
24. Sosna J, Pedrosa I, Dewolf WC, et al. MR imaging of the prostate at 3 Tesla: comparison of an external phased-array coil to imaging with an endorectal coil at 1.5 Tesla. Acad Radiol 2004;11(8): 857–62. [PubMed: 15354305]
25. Turkbey B, Merino MJ, Gallardo EC, et al. Comparison of endorectal coil and nonendorectal coil T2W and diffusion-weighted MRI at 3 Tesla for localizing prostate cancer: correlation with whole-mount histopathology. J Magn Reson Imaging 2014;39(6): 1443–8. [PubMed: 24243824]
26. Daniel BL, Shimakawa A, Blum MR, et al. Single-shot fluid attenuated inversion recovery (FLAIR) magnetic resonance imaging of the bladder.J Magn Reson Imaging 2000;11(6):673–7. [PubMed: 10862067]
27. Kier R, Wain S, Troiano R. Fast spin-echo MR images of the pelvis obtained with a phased-array coil: value in localizing and staging prostatic carcinoma. AJR Am J Roentgenol 1993;161(3):601–6. [PubMed: 8352116]
28. Liney GP, Knowles AJ, Manton DJ, et al. Comparison of conventional single echo and multi-echo sequences with a fast spin-echo sequence for quantitative T2 mapping: application to the prostate. J Magn Reson Imaging 1996;6(4):603–7. [PubMed: 8835953]
29. Itatani R, Namimoto T, Takaoka H, et al. Extracapsular extension of prostate cancer: diagnostic value of combined multiparametric magnetic resonance imaging and isovoxel 3-dimensional T2-weighted imaging at 1.5 T. J Comput Assist Tomogr 2015;39(1):37–43. [PubMed: 25340587]
30. Yamauchi FI, Penzkofer T, Fedorov A, et al. Prostate cancer discrimination in the peripheral zone with a reduced field-of-view T2-mapping MRI sequence. Magn Reson Imaging 2015;33(5):525–30. [PubMed: 25687187]
31. Treier R, Steingoetter A, Fried M, et al. Optimized and combined T1 and B1 mapping technique for fast and accurate T1 quantification in contrastenhanced abdominal MRI. Magn Reson Med 2007;57(3):568–76. [PubMed: 17326175]
32. McMahon CJ, Bloch BN, Lenkinski RE, et al. Dynamic contrast-enhanced MR imaging in the evaluation of patients with prostate cancer. Magn Reson Imaging Clin N Am 2009;17(2):363–83. [PubMed: 19406364]
33. de Bazelaire C, Rofsky NM, Duhamel G, et al. Combined T2* and T1 measurements for improved perfusion and permeability studies in high field using dynamic contrast enhancement. Eur Radiol 2006;16(9):2083–91. [PubMed: 16583215]
34. El-Diasty T, Mansour O, Farouk A. Diuretic contrast-enhanced magnetic resonancephy versus intravenous urography for depiction of nondilated urinary tracts. Abdom Imaging 2003;28(1):135–45. [PubMed: 12483401]
35. Ergen FB, Hussain HK, Carlos RC, et al. 3D excretory MR urography: improved image quality with intravenous saline and diuretic administration. J Magn Reson Imaging 2007;25(4):783–9. [PubMed: 17335024]
36. Hagspiel KD, Butty S, Nandalur KR, et al. Magnetic resonance urography for the assessment of potential renal donors: comparison of the RARE technique with a low-dose gadolinium-enhanced magnetic resonance urography technique in the absence of pharmacological and mechanical intervention. Eur Radiol 2005;15(11):2230–7. [PubMed: 16021454]
37. Kim B, Semelka RC, Ascher SM, et al. Bladder tumor staging: comparison of contrast-enhanced CT, T1- and T2-weighted MR imaging, dynamic gadolinium-enhanced imaging, and late gadolinium-enhanced imaging. Radiology 1994; 193(1):239–45. [PubMed: 8090898]

38. Barentsz JO, Jager GJ, van Vierzen PB, et al. Staging urinary bladder cancer after transurethral biopsy: value of fast dynamic contrast-enhanced MR imaging. Radiology 1996;201(1):185–93. [PubMed: 8816542]
39. Verma S, Turkbey B, Muradyan N, et al. Overview of dynamic contrast-enhanced MRI in prostate cancer diagnosis and management. AJR Am J Roentgenol 2012;198(6):1277–88. [PubMed: 22623539]
40. Rosenkrantz AB, Geppert C, Grimm R, et al. Dynamic contrast-enhanced MRI of the prostate with high spatiotemporal resolution using compressed sensing, parallel imaging, and continuous golden-angle radial sampling: preliminary experience. Magn Reson Imaging 2015;41(5):1365–73.
41. Tofts PS, Brix G, Buckley DL, et al. Estimating kinetic parameters from dynamic contrast-weighted MRI of a diffusable tracer: standardized quantities and symbols. J Magn Reson Imaging 1999;10(3):223–32. [PubMed: 10508281]
42. Bloch BN, Genega EM, Costa DN, et al. Prediction of prostate cancer extracapsular extension with high spatial resolution dynamic contrast-enhanced 3-T MRI. Eur Radiol 2012;22(10): 2201–10. [PubMed: 22661019]
43. Skare S, Newbould RD, Clayton DB, et al. Clinical multishot DW-EPI through parallel imaging with considerations of susceptibility, motion, and noise. Magn Reson Med 2007;57(5):881–90. [PubMed: 17457876]
44. Barentsz JO, Richenberg J, Clements R, et al. ESUR prostate MR guidelines 2012. Eur Radiol 2012;22(4):746–57. [PubMed: 22322308]
45. Kim CK, Park BK, Kim B. High-b-value diffusion-weighted imaging at 3 T to detect prostate cancer: comparisons between b values of 1,000 and 2,000 s/mm2. AJR Am J Roentgenol 2010; 194(1):W33–7. [PubMed: 20028888]
46. Katahira K, Takahara T, Kwee TC, et al. Ultra-highb-value diffusion-weighted MR imaging for the detection of prostate cancer: evaluation in 201 cases with histopathological correlation. Eur Radiol 2011;21(1):188–96. [PubMed: 20640899]
47. Ohgiya Y, Suyama J, Seino N, et al. Diagnostic accuracy of ultra-high-b-value 3.0-T diffusion-weighted MR imaging for detection of prostate cancer. Clin Imaging 2012;36(5):526–31. [PubMed: 22920357]
48. Rosen Y, Bloch BN, Lenkinski RE, et al. 3T MR of the prostate: reducing susceptibility gradients by inflating the endorectal coil with a barium sulfate suspension. Magn Reson Med 2007;57(5): 898–904. [PubMed: 17457870]
49. Scherrer B, Gholipour A, Warfield SK. Super-resolution reconstruction to increase the spatial resolution of diffusion weighted images from orthogonal anisotropic acquisitions. Med Image Anal 2012; 16(7):1465–76. [PubMed: 22770597]
50. Donato F, Jr, Costa DN, Yuan Q, et al. Geometric distortion in diffusion-weighted MR imaging of the prostate-contributing factors and strategies for improvement. Acad Radiol 2014;21(6): 817–23. [PubMed: 24709379]
51. Alsop DC, Detre JA. Multisection cerebral blood flow MR imaging with continuous arterial spin labeling. Radiology 1998;208(2):410–6. [PubMed: 9680569]
52. Fenchel M, Martirosian P, Langanke J, et al. Perfusion MR imaging with FAIR true FISP spin labeling in patients with and without renal artery stenosis: initial experience. Radiology 2006; 238(3):1013–21. [PubMed: 16439565]
53. Lanzman RS, Wittsack HJ, Martirosian P, et al. Quantification of renal allograft perfusion using arterial spin labeling MRI: initial results. Eur Radiol 2010;20(6):1485–91. [PubMed: 19949799]
54. Martirosian P, Klose U, Mader I, et al. FAIR trueFISP perfusion imaging of the kidneys. Magn Reson Med 2004;51(2):353–61. [PubMed: 14755661]
55. Ogawa S, Lee TM, Nayak AS, et al. Oxygenation- sensitive contrast in magnetic resonance image of rodent brain at high magnetic fields. Magn Reson Med 1990;14(1):68–78. [PubMed: 2161986]
56. Prasad PV, Edelman RR, Epstein FH. Noninvasive evaluation of intrarenal oxygenation with BOLD MRI. Circulation 1996;94(12):3271–5. [PubMed: 8989140]
57. Choi YA, Kim CK, Park SY, et al. Subtype differentiation of renal cell carcinoma using diffusion-weighted and blood oxygenation level-dependent MRI. AJR Am J Roentgenol 2014;203(1):W78–84. [PubMed: 24951231]

58. Min JH, Kim CK, Park BK, et al. Assessment of renal lesions with blood oxygenation level-dependent MRI at 3 T: preliminary experience. AJR Am J Roentgenol 2011;197(3):W489–94. [PubMed: 21862777]
59. Katz-Brull R, Rofsky NM, Morrin MM, et al. Decreases in free cholesterol and fatty acid unsaturation in renal cell carcinoma demonstrated by breath-hold magnetic resonance spectroscopy. Am J Physiol Renal Physiol 2005;288(4):F637–41. [PubMed: 15572523]
60. Tugnoli V, Bottura G, Fini G, et al. 1H-NMR and 13C-NMR lipid profiles of human renal tissues. Biopolymers 2003;72(2):86–95. [PubMed: 12583011]
61. Costello LC, Franklin RB. Concepts of citrate production and secretion by prostate. 1. Metabolic relationships. Prostate 1991;18(1):25–46. [PubMed: 1987578]
62. Costello LC, Franklin RB. Concepts of citrate production and secretion by prostate: 2. Hormonal relationships in normal and neoplastic prostate. Prostate 1991;19(3):181–205. [PubMed: 1946039]
63. Kahn T, Bürrig K, Schmitz-Dräger B, et al. Prostatic carcinoma and benign prostatic hyperplasia: MR imaging with histopathologic correlation. Radiology 1989;173(3):847–51. [PubMed: 2479050]
64. Kurhanewicz J, Swanson MG, Nelson SJ, et al. Combined magnetic resonance imaging and spectroscopic imaging approach to molecular imaging of prostate cancer. J Magn Reson Imaging 2002; 16(4):451–63. [PubMed: 12353259]
65. Motzer RJ, Hutson TE, Tomczak P, et al. Sunitinib versus interferon alfa in metastatic renal-cell carcinoma. N Engl J Med 2007;356(2):115–24. [PubMed: 17215529]
66. Schrader AJ, Olbert PJ, Hegele A, et al. Metastatic non-clear cell renal cell carcinoma: current therapeutic options. BJU Int 2008;101(11):1343–5. [PubMed: 18241246]
67. Bostwick DG, Murphy GP. Diagnosis and prognosis of renal cell carcinoma: highlights from an international consensus workshop. Semin Urol Oncol 1998;16(1):46–52. [PubMed: 9508083]
68. Leroy X, Zini L, Leteurtre E, et al. Morphologic subtyping of papillary renal cell carcinoma: correlation with prognosis and differential expression of MUC1 between the two subtypes. Mod Pathol 2002; 15(11):1126–30. [PubMed: 12429790]
69. Pedrosa I, Chou MT, Ngo L, et al. MR classification of renal masses with pathologic correlation. Eur Radiol 2008;18(2):365–75. [PubMed: 17899106]
70. Sun MR, Ngo L, Genega EM, et al. Renal cell carcinoma: dynamic contrast-enhanced MR imaging for differentiation of tumor subtypes–correlation with pathologic findings. Radiology 2009;250(3): 793–802. [PubMed: 19244046]
71. Lanzman RS, Robson PM, Sun MR, et al. Arterial spin-labeling MR imaging of renal masses: correlation with histopathologic findings. Radiology 2012; 265(3):799–808. [PubMed: 23047841]
72. Roy C, Sr, El Ghali S, Buy X, et al. Significance of the pseudocapsule on MRI of renal neoplasms and its potential application for local staging: a retrospective study. AJR Am J Roentgenol 2005; 184(1):113–20. [PubMed: 15615960]
73. Mejean A, Hopirtean V, Bazin JP, et al. Prognostic factors for the survival of patients with papillary renal cell carcinoma: meaning of histological typing and multifocality. J Urol 2003;170(3):764–7. [PubMed: 12913693]
74. Sasiwimonphan K, Takahashi N, Leibovich BC, et al. Small (<4 cm) renal mass: differentiation of angiomyolipoma without visible fat from renal cell carcinoma utilizing MR imaging. Radiology 2012; 263(1):160–8. [PubMed: 22344404]
75. Rosenkrantz AB, Sekhar A, Genega EM, et al. Prognostic implications of the magnetic resonance imaging appearance in papillary renal cell carcinoma. Eur Radiol 2013;23(2):579–87. [PubMed: 22903703]
76. Eisenhauer EA, Therasse P, Bogaerts J, et al. New response evaluation criteria in solid tumours: revised RECIST guideline (version 1.1). Eur J Cancer 2009;45(2):228–47. [PubMed: 19097774]
77. Baccala A, Jr, Hedgepeth R, Kaouk J, et al. Pathological evidence of necrosis in recurrent renal mass following treatment with sunitinib. Int J Urol 2007; 14(12):1095–7 [discussion: 1097]. [PubMed: 18036049]
78. Ratain MJ, Eckhardt SG. Phase II studies of modern drugs directed against new targets: if you are fazed, too, then resist RECIST. J Clin Oncol 2004; 22(22):4442–5. [PubMed: 15483011]

79. Rosen MA, Schnall MD. Dynamic contrast-enhanced magnetic resonance imaging for assessing tumor vascularity and vascular effects of targeted therapies in renal cell carcinoma. Clin Cancer Res 2007;13(2 Pt 2):770s–6s. [PubMed: 17255308]
80. van der Veldt AA, Meijerink MR, van den Eertwegh AJ, et al. Targeted therapies in renal cell cancer: recent developments in imaging. Target Oncol 2010;5(2):95–112. [PubMed: 20625845]
81. Hahn OM, Yang C, Medved M, et al. Dynamic contrast-enhanced magnetic resonance imaging pharmacodynamic biomarker study of sorafenib in metastatic renal carcinoma. J Clin Oncol 2008; 26(28):4572–8. [PubMed: 18824708]
82. Wolf RL, Wang J, Wang S, et al. Grading of CNS neoplasms using continuous arterial spin labeled perfusion MR imaging at 3 Tesla. J Magn Reson Imaging 2005;22(4):475–82. [PubMed: 16161080]
83. de Bazelaire C, Alsop DC, George D, et al. Magnetic resonance imaging-measured blood flow change after antiangiogenic therapy with PTK787/ ZK 222584 correlates with clinical outcome in metastatic renal cell carcinoma. Clin Cancer Res 2008; 14(17):5548–54. [PubMed: 18765547]
84. Akita H, Jinzaki M, Kikuchi E, et al. Preoperative T categorization and prediction of histopathologic grading of urothelial carcinoma in renal pelvis using diffusion-weighted MRI. AJR Am J Roentgenol 2011;197(5):1130–6. [PubMed: 22021505]
85. Shokeir AA, El-Diasty T, Eassa W, et al. Diagnosis of ureteral obstruction in patients with compromised renal function: the role of noninvasive imaging modalities. J Urol 2004;171(6 Pt 1): 2303–6. [PubMed: 15126809]
86. Shokeir AA, El-Diasty T, Eassa W, et al. Diagnosis of noncalcareous hydronephrosis: role of magnetic resonance urography and noncontrast computed tomography. Urology 2004;63(2):225–9. [PubMed: 14972458]
87. Weeks SM, Brown ED, Brown JJ, et al. Transitional cell carcinoma of the upper urinary tract: staging by MRI. Abdom Imaging 1995;20(4):365–7. [PubMed: 7549745]
88. O'Connor OJ, McLaughlin P, Maher MM. MR urography. AJR Am J Roentgenol 2010;195(3):W201–6. [PubMed: 20729416]
89. Browne RF, Meehan CP, Colville J, et al. Transitional cell carcinoma of the upper urinary tract: spectrum of imaging findings. Radiographics 2005;25(6): 1609–27. [PubMed: 16284138]
90. Obuchi M, Ishigami K, Takahashi K, et al. Gadolinium-enhanced fat-suppressed T1-weighted imaging for staging ureteral carcinoma: correlation with histopathology. AJR Am J Roentgenol 2007; 188(3):W256–61. [PubMed: 17312032]
91. Uchida Y, Yoshida S, Kobayashi S, et al. Diffusion- weighted MRI as a potential imaging biomarker reflecting the metastatic potential of upper urinary tract cancer. Br J Radiol 2014;87(1042):20130791. [PubMed: 25074719]
92. Yoshida S, Kobayashi S, Koga F, et al. Apparent diffusion coefficient as a prognostic biomarker of upper urinary tract cancer: a preliminary report. Eur Radiol 2013;23(8):2206–14. [PubMed: 23494496]
93. Takeuchi M, Sasaki S, Ito M, et al. Urinary bladder cancer: diffusion-weighted MR imaging–accuracy for diagnosing T stage and estimating histologic grade. Radiology 2009;251(1):112–21. [PubMed: 19332849]
94. Watanabe H, Kanematsu M, Kondo H, et al. Preoperative T staging of urinary bladder cancer: does diffusion-weighted MRI have supplementary value? AJR Am J Roentgenol 2009;192(5):1361–6. [PubMed: 19380561]
95. Tanimoto A, Yuasa Y, Imai Y, et al. Bladder tumor staging: comparison of conventional and gadolinium-enhanced dynamic MR imaging and CT. Radiology 1992;185(3):741–7. [PubMed: 1438756]
96. Matsuki M, Inada Y, Tatsugami F, et al. Diffusion- weighted MR imaging for urinary bladder carcinoma: initial results. Eur Radiol 2007;17(1):201–4. [PubMed: 16865369]
97. El-Assmy A, Abou-El-Ghar ME, Mosbah A, et al. Bladder tumour staging: comparison of diffusion- and T2-weighted MR imaging. Eur Radiol 2009; 19(7):1575–81. [PubMed: 19247665]
98. Takeuchi M, Sasaki S, Naiki T, et al. MR imaging of urinary bladder cancer for T-staging: a review and a pictorial essay of diffusion-weighted imaging. J Magn Reson Imaging 2013;38(6):1299–309. [PubMed: 24265260]

99. Kobayashi S, Koga F, Kajino K, et al. Apparent diffusion coefficient value reflects invasive and proliferative potential of bladder cancer. J Magn Reson Imaging 2014;39(1):172–8. [PubMed: 23589321]
100. Margulis V, Lotan Y, Karakiewicz PI, et al. Multi-institutional validation of the predictive value of Ki-67 labeling index in patients with urinary bladder cancer. J Natl Cancer Inst 2009;101(2):114–9. [PubMed: 19141773]
101. Margulis V, Shariat SF, Ashfaq R, et al. Ki-67 is an independent predictor of bladder cancer outcome in patients treated with radical cystectomy for organ-confined disease. Clin Cancer Res 2006; 12(24):7369–73. [PubMed: 17189409]
102. Yoshida S, Koga F, Kobayashi S, et al. Role of diffusion-weighted magnetic resonance imaging in predicting sensitivity to chemoradiotherapy in muscle-invasive bladder cancer. Int J Radiat Oncol Biol Phys 2012;83(1):e21–7. [PubMed: 22414281]
103. Tuncbilek N, Kaplan M, Altaner S, et al. Value of dynamic contrast-enhanced MRI and correlation with tumor angiogenesis in bladder cancer. AJR Am J Roentgenol 2009;192(4):949–55. [PubMed: 19304699]
104. Cornud F, Delongchamps NB, Mozer P, et al. Value of multiparametric MRI in the work-up of prostate cancer. Curr Urol Rep 2012;13(1):82–92. [PubMed: 22139624]
105. Kurhanewicz J, Vigneron D, Carroll P, et al. Multiparametric magnetic resonance imaging in prostate cancer: present and future. Curr Opin Urol 2008;18(1):71–7. [PubMed: 18090494]
106. Labanaris AP, Zugor V, Takriti S, et al. The role of conventional and functional endorectal magnetic resonance imaging in the decision of whether to preserve or resect the neurovascular bundles during radical retropubic prostatectomy. Scand J Urol Nephrol 2009;43(1):25–31. [PubMed: 18759166]
107. Sciarra A, Barentsz J, Bjartell A, et al. Advances in magnetic resonance imaging: how they are changing the management of prostate cancer. Eur Urol 2011;59(6):962–77. [PubMed: 21367519]
108. Muller BG, van den Bos W, Pinto PA, et al. Imaging modalities in focal therapy: patient selection, treatment guidance, and follow-up. Curr Opin Urol 2014;24(3):218–24. [PubMed: 24637316]
109. Sonn GA, Chang E, Natarajan S, et al. Value of targeted prostate biopsy using magnetic resonance-ultrasound fusion in men with prior negative biopsy and elevated prostate-specific antigen. Eur Urol 2014;65(4):809–15. [PubMed: 23523537]
110. Zhang ZX, Yang J, Zhang CZ, et al. The value of magnetic resonance imaging in the detection of prostate cancer in patients with previous negative biopsies and elevated prostate-specific antigen levels: a meta-analysis. Acad Radiol 2014;21(5): 578–89. [PubMed: 24703470]
111. Mendhiratta N, Rosenkrantz AB, Meng X, et al. MRI-ultrasound fusion-targeted prostate biopsy in a consecutive cohort of men with no previous biopsy: reduction of over-detection through improved risk stratification. J Urol 2015 [Epub ahead of print].
112. Hoeks CM, Barentsz JO, Hambrock T, et al. Prostate cancer: multiparametric MR imaging for detection, localization, and staging. Radiology 2011; 261(1):46–66. [PubMed: 21931141]
113. Hricak H, Choyke PL, Eberhardt SC, et al. Imaging prostate cancer: a multidisciplinary perspective. Radiology 2007;243(1):28–53. [PubMed: 17392247]
114. Hambrock T, Somford DM, Huisman HJ, et al. Relationship between apparent diffusion coefficients at 3.0-T MR imaging and Gleason grade in peripheral zone prostate cancer. Radiology 2011;259(2):453–61. [PubMed: 21502392]
115. Vargas HA, Akin O, Franiel T, et al. Diffusion- weighted endorectal MR imaging at 3 T for prostate cancer: tumor detection and assessment of aggressiveness. Radiology 2011;259(3):775–84. [PubMed: 21436085]
116. van As NJ, de Souza NM, Riches SF, et al. A study of diffusion-weighted magnetic resonance imaging in men with untreated localised prostate cancer on active surveillance. Eur Urol 2009;56(6):981–7. [PubMed: 19095345]
117. Giles SL, Morgan VA, Riches SF, et al. Apparent diffusion coefficient as a predictive biomarker of prostate cancer progression: value of fast and slow diffusion components. AJR Am J Roentgenol 2011;196(3):586–91. [PubMed: 21343500]
118. Sistrom CL, Langlotz CP. A framework for improving radiology reporting. J Am Coll Radiol 2005;2(2):159–67. [PubMed: 17411786]

119. Dickinson L, Ahmed HU, Allen C, et al. Scoring systems used for the interpretation and reporting of multiparametric MRI for prostate cancer detection, localization, and characterization: could standardization lead to improved utilization of imaging within the diagnostic pathway? J Magn Reson Imaging 2013;37(1):48–58. [PubMed: 22566285]

120. Rosenkrantz AB, Haghighi M, Horn J, et al. Utility of quantitative MRI metrics for assessment of stage and grade of urothelial carcinoma of the bladder: preliminary results. AJR Am J Roentgenol 2013; 201(6):1254–9. [PubMed: 24261364]

121. Muller BG, Shih JH, Sankineni S, et al. Prostate cancer: interobserver agreement and accuracy with the revised prostate imaging reporting and data system at multiparametric MR imaging. Radiology 2015;142818.

KEY POINTS

- Multiparametric MR imaging (mpMRI) protocols include standard sequences tailored for the morphologic evaluation of urogenital tract malignancies that take into account specific needs, such as spatial resolution, respiratory compensation strategies versus breath-hold imaging, and anatomic coverage.
- mpMRI also includes acquisitions that provide information about the tumor microenvironment and that extend beyond their morphologic assessment, such as diffusion-weighted imaging (DWI), dynamic contrast-enhanced (DCE) MR imaging, and arterial spin-labeled (ASL) strategies.
- mpMRI may offer detailed preoperative insight into renal cell carcinoma (RCC) histologic subtype and grade and provide an opportunity to quantitatively assess tumor response to targeted therapies in patients with metastatic disease.
- DWI and apparent diffusion coefficient (ADC) values may play a role in predicting histologic grade and potential treatment response of urothelial carcinoma.
- The role of mpMRI in the evaluation of prostate cancer extends beyond tumor staging and now includes disease identification/localization prior to targeted biopsy as well as follow-up of patients on active surveillance.

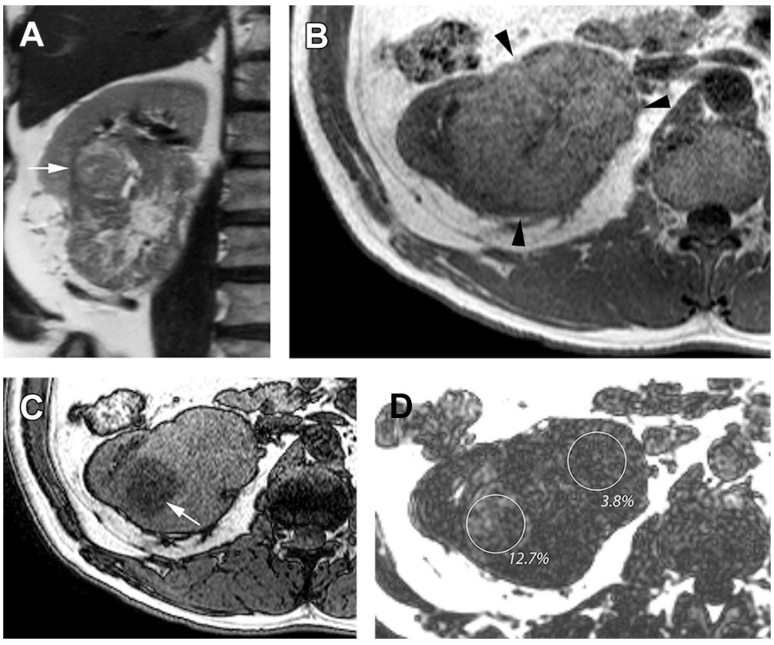

Fig. 1.

Heterogeneous lipid accumulation in high-grade clear cell renal cell carcinoma (Fuhrman grade 3). (*A*) Coronal T2-weighted SSTSE image shows a large hetero-geneous right renal mass with a more focal nodule in the superolateral aspect of the mass (*arrow*). (*B*) Axial T1-weighted in-phase gradient-echo image through the level of the nodule (*A*) shows near-uniform moderately hyperintense signal intensity relative to renal cortex in the mass (*arrowheads*). (*C*) Axial T1-weighted gradient-echo opposed-phase image, at the same anatomic level as in (*B*), shows marked diffuse drop in signal intensity in the region well defined nodule (*arrow*), indicating the presence of intravoxel fat. (*D*) Fat fraction map calculated from a 3-D T1-weighted, multiecho, multipoint Dixon technique confirms and quantifies the presence of intravoxel fat within the mass. Note the high fat fraction (12.7%) in the nodule compared with the lower fat level in rest of the mass (3.8%). The tumor showed histopathologic features consistent with the presence of greater fat content within the nodule.

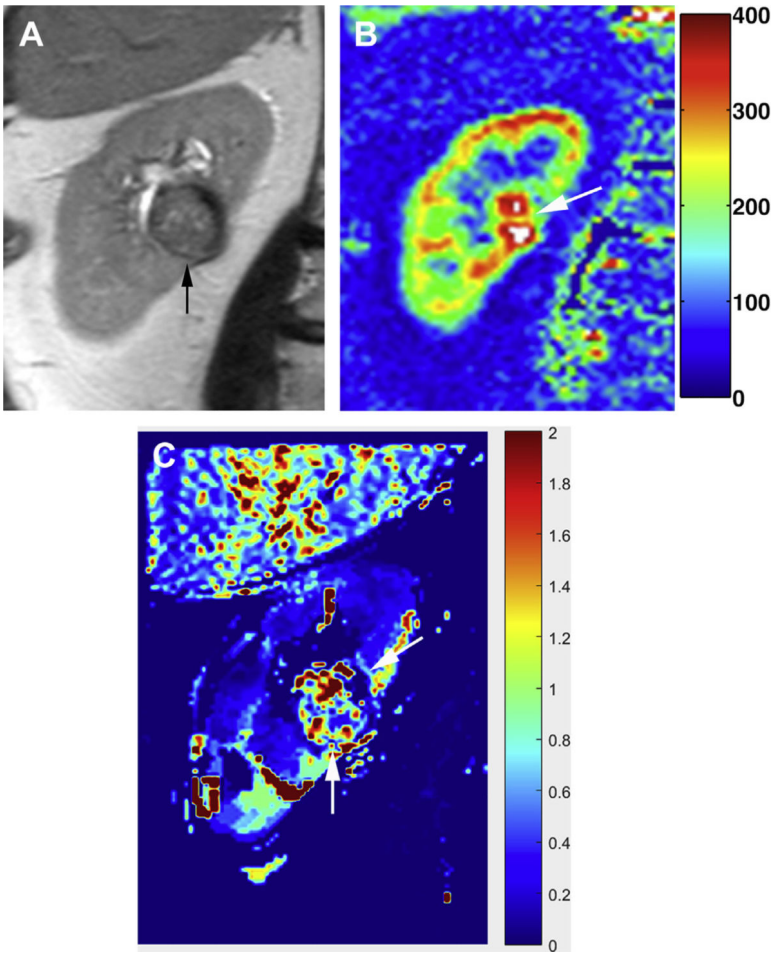

Fig. 2.

Low-grade (Fuhrman grade 2). (*A*) Coronal T2-weighted SSTSE image shows a central, partially exophytic mass (*arrow*), heterogeneously isointense to hypointense to renal cortex, arising from the mid–right kidney. (*B*) ASL perfusion map shows high levels of perfusion (ie, >300 mL/100 g/min) within the mass (*arrow*). (*C*) K^{trans} map generated from a DCE acquisition confirms high vascularity in the mass (*arrows*).

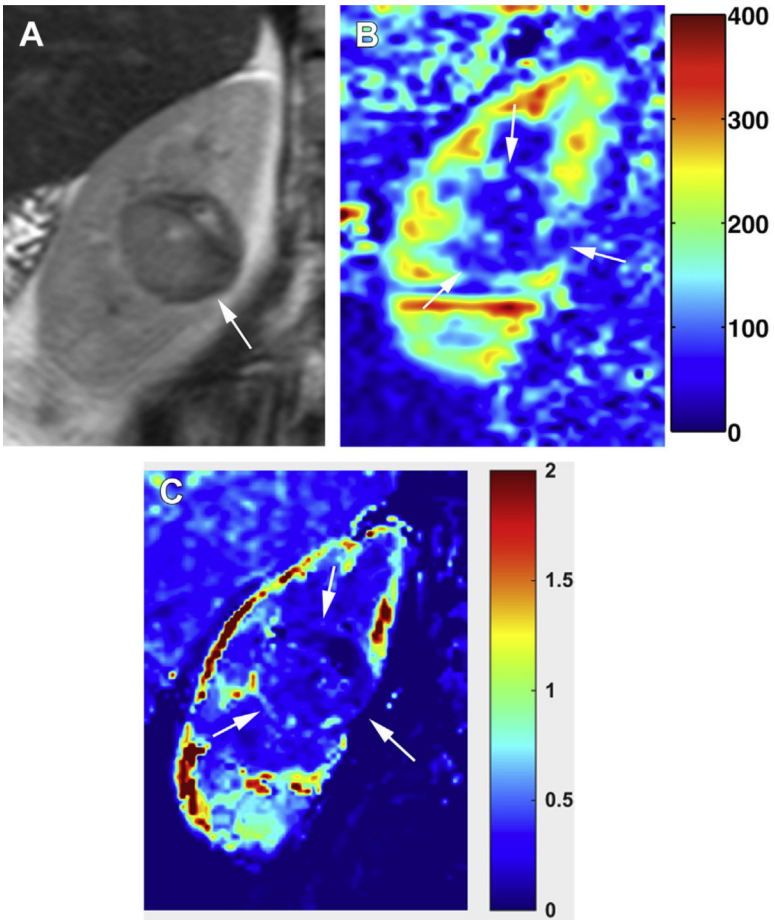

Fig. 3.

Papillary renal cell carcinoma (Fuhrman grade 3). (*A*) Coronal T2-weighted SSTSE image shows a hypointense renal mass (*arrow*) in the central, mid–right kidney. (*B*) ASL perfusion map shows low levels of perfusion in the mass (*arrows*). (*C*) K^{trans} map generated from DCE acquisition demonstrate expected hypovascularity within the mass (*arrows*).

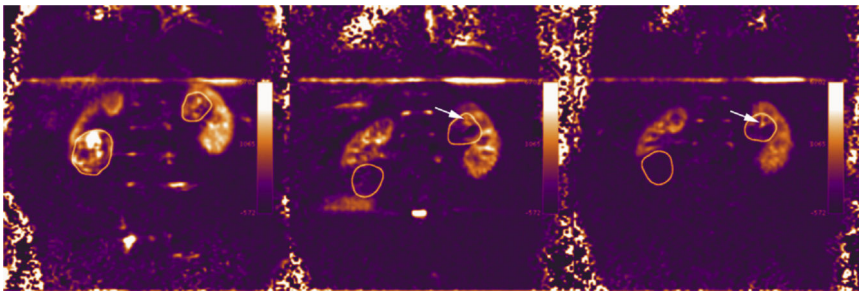

Fig. 4.

Coronal ASL MR imaging images at baseline (*left*), and at 2 weeks (*center*), and after (*right*) the second cycle of therapy with sunitinib in a patient with mRCC. Note the hypervascular nature of the right and left renal masses (*circles*) showing high signal (ie, blood flow) on the ASL image at baseline. The right mass showed progressive decrease in size at 2 weeks of (28%) and after the second cycle (40%) on anatomic T2-weighted images (not shown) and marked decrease in tumor perfusion with 82% and 93% decrease at these time points, respectively. The left renal mass showed a less pronounced decrease in size (6.5% and 20% decrease at 2 weeks and after the second cycle, respectively). Note some persistent central perfusion in the left renal mass (*arrows*) indicative of lack of response in that portion of the tumor.

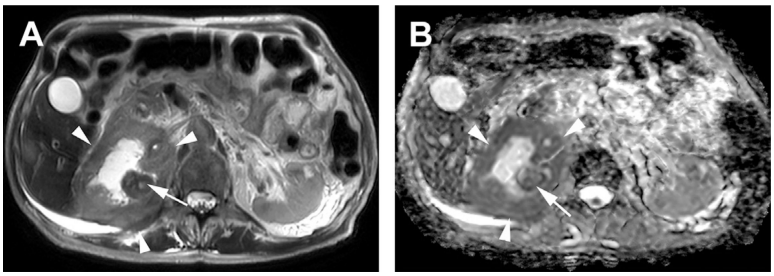

Fig. 5.

Upper tract urothelial carcinoma. (*A*) Axial T2-weighted SSTSE image of the upper abdomen shows a large, infiltrative mass encompassing the right renal collecting system (arrowheads) with a more focal, peripheral nodular component (*arrow*). (*B*) Axial ADC image shows restricted diffusion in the mass (*arrowheads*) and nodule (*arrow*). Biopsy confirmed high-grade urothelial carcinoma.

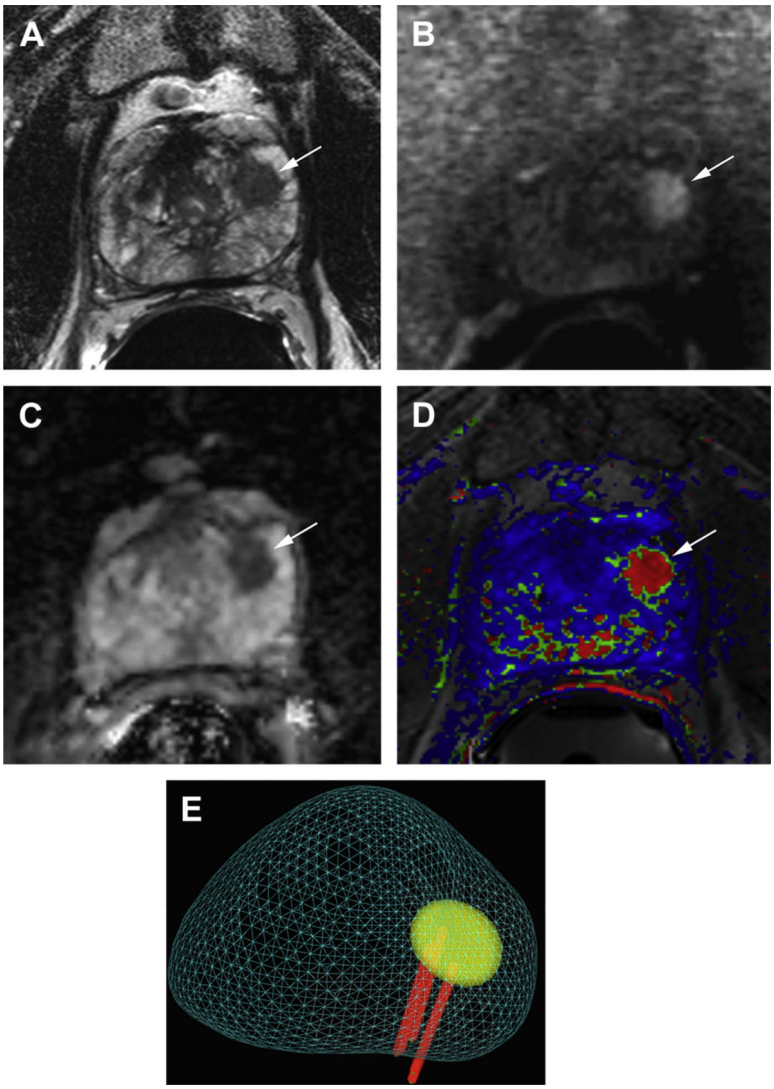

Fig. 6.

Prostate cancer diagnosed with mpMRI and targeted MR imaging–TRUS fusion biopsy. A 57-yearold man with elevated PSA (11 ng/mL) and 2 previous negative biopsies underwent MR imaging for biopsy planning. (*A*) Axial T2-weighted image shows a focal area of low signal intensity in the anterior left midgland (*arrow*). (*B*) The lesion shows restricted diffusion manifested by high signal intensity (*arrow*) on the DWI (b-value = 2000) and (*C*) low signal intensity (arrow) on the ADC map as well as rapid enhancement and washout on DCE, (*D*) illustrated by red color (arrow) on the kinetic map. (*E*) Targeted MR imaging–TRUS fusion biopsy revealed Gleason score 3 + 4 prostate cancer in 5 of 5 cores with up to 55% of core length involved by tumor.

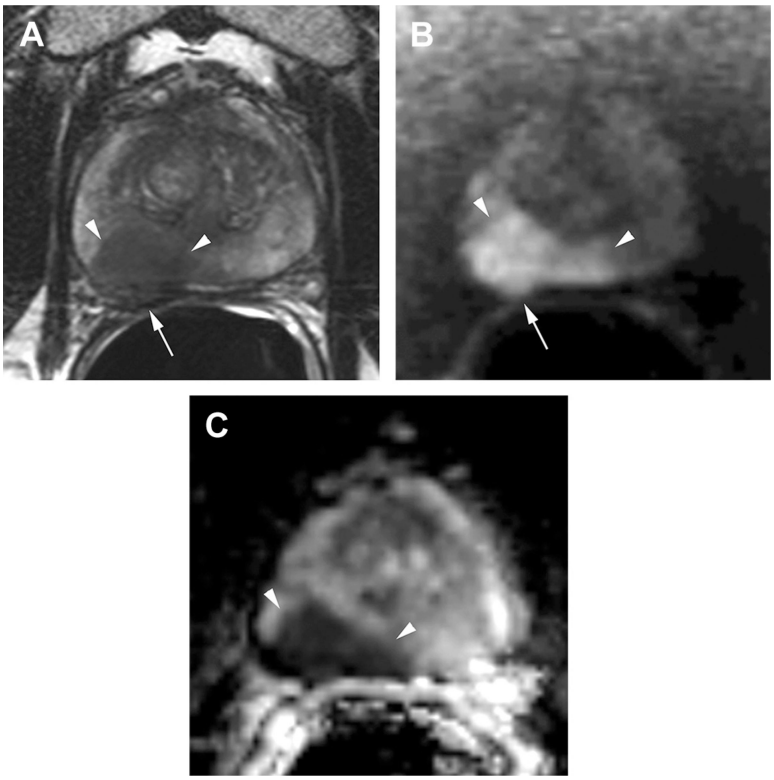

Fig. 7.

Inverse relationship between ADC values and Gleason score. A 64-year-old man with elevated PSA (36 ng/mL) and recently diagnosed prostate cancer underwent MR imaging for local staging. (*A*) Axial T2-weighted image shows a large, ill-defined mass predominantly involving the right midgland peripheral zone (*arrowheads*). (*B*) The mass exhibits marked increased signal intensity (*arrowheads*) on the diffusion image (b-value = 2000). Note the larger tumor extension demonstrated by DWI compared with the T2-weighted image. Posterior bulging of the prostate contour on both T2- and diffusion-weighted images (*arrows* in [*A*] and [*B*]) is consistent with extraprostatic extension. (*C*) The ADC map confirms marked restriction in the mass (*arrowheads*) with low ADC values (0.5 10^{-3} mm^2/s), which increases the risk of high Gleason score (ie, aggressive tumor) in this patient. Biopsy confirmed the presence of clinically significant cancer with Gleason score 4 + 3 prostate cancer in 4 cores of the right midgland with up to 95% of core length involved by tumor.